





A Decade of Electrocatalysis with Metal Aerogels: A Perspective

Weishan Li ¹, Beibei Weng ¹, Xiaoyue Sun ¹ , Bin Cai ^{2,*} , René Hübner ³ , Yunjun Luo ¹  and Ran Du ^{1,*}

¹ School of Materials Science and Engineering, Key Laboratory of High Energy Density Materials of the Ministry of Education, Beijing Institute of Technology, Beijing 100081, China

² School of Chemistry and Chemical Engineering, Shandong University, Jinan 250100, China

³ Helmholtz-Zentrum Dresden-Rossendorf, Institute of Ion Beam Physics and Materials Research, Bautzner Landstrasse 400, 01328 Dresden, Germany

* Correspondence: bin.cai@sdu.edu.cn (B.C.); rdu@bit.edu.cn (R.D.)

Abstract: Nowadays, great efforts have been spent on addressing concerns over energy and environmental crises. Among these efforts, electrocatalysis is widely recognized and studied for its high efficiency and easy processability. As a class of emerging electrocatalysts, metal aerogels (MAs) stand out in the last decade. In virtue of their three-dimensional conductive pathways, their library of catalytically/optically active sites, and their robust network structures, MAs have unique advantages in electrocatalysis. However, due to the short history of MAs, there is insufficient research on them, leaving significant room for material design and performance optimization. This perspective will mainly focus on electrocatalysis with MAs, aiming to summarize the state-of-the-art progress and to guide the on-target design of efficient MAs-based electrocatalysts towards energy- and environment-related applications.

Keywords: electrocatalysis; metal aerogels; sol-gel; nanostructures; porous materials

1. Introduction

Electrocatalysis plays a critical role in diverse energy- and environment-related processes, such as the oxygen reduction reaction (ORR) and the fuel oxidation reaction (e.g., the alcohol oxidation reaction (AOR) and the hydrogen oxidation reaction (HOR)) in fuel cells [1–4], the oxygen evolution reaction (OER) and the hydrogen evolution reaction (HER) in water splitting [5–7], and the carbon dioxide reduction reaction (CO₂RR) in producing high value-added chemicals [8,9]. Besides a high efficiency, the electrochemical process can flexibly utilize the stored electricity generated from renewable energy, thus alleviating the energy crisis resulting from the excessive use of fossil fuels. Therefore, to promote these electrochemical processes, the development of high-performance electrocatalysts is central for both the scientific and the industrial community.

In principle, efficient electrocatalysis calls for abundant accessible active sites, high single-site activity, high electrical conductivity, and reasonable cost. In the past several decades, a wide range of materials, including metals, metallic compounds (e.g., metal oxides and metal dichalcogenides), nanocarbons, and various composites, have been extensively investigated as electrocatalysts [10–16]. In particular, nanostructuring can endow original bulk materials with a large specific surface area (SSA), high reactivity, and dramatic size effects, thus promoting their performance. While significant advances have been achieved in the creative synthesis of nanomaterials, the intrinsic instability of this nano-sized matter and the relatively poor electrical connection pose difficulties in achieving high-performance and robust electrocatalysis. In this regard, the exploration of new catalysts is of paramount importance.

Metal aerogels (MAs), a new class of porous materials developed in 2009 [17,18], are promising for addressing the aforementioned issues. As these aerogels are entirely built up by nanostructured metals, MAs inherit the unique physicochemical properties of metals



Citation: Li, W.; Weng, B.; Sun, X.; Cai, B.; Hübner, R.; Luo, Y.; Du, R. A Decade of Electrocatalysis with Metal Aerogels: A Perspective. *Catalysts* **2023**, *13*, 167. <https://doi.org/10.3390/catal13010167>

Academic Editor: Carlo Santoro

Received: 17 October 2022

Revised: 24 December 2022

Accepted: 9 January 2023

Published: 10 January 2023



Copyright: © 2023 by the authors. Licensee MDPI, Basel, Switzerland. This article is an open access article distributed under the terms and conditions of the Creative Commons Attribution (CC BY) license (<https://creativecommons.org/licenses/by/4.0/>).

(e.g., catalytic activity, electrical conductivity, and special optical properties) and structural features of aerogels (e.g., porous network, large SSA, and monolithic architecture) [19,20]. In this light, featuring numerous active sites, rapid mass/electron transfer pathways, robust structure, and tunable compositions, MAs manifest unprecedented potential as highly active and durable electrocatalysts, overwhelming conventional non-metal and unsupported metallic catalysts [21]. Despite these unique attributes, the development of MAs has not been smooth, particularly in their early years, which can be attributed to an insufficient materials basis resulting from their unconventional formation behavior, immature fabrication methods, and less-explored physicochemical properties [22,23]. In this regard, the corresponding application studies, such as those for electrocatalysis, have inevitably been slowed down. Although quite a few synthesized MAs have been proven to efficiently catalyze diverse electrochemical processes [22–25], their design principles are not clear, and their performance needs further improvement.

In the past few years, several reviews have summarized the controlled synthesis of MAs and/or their analogs, as well as their diverse applications [19,26,27]. However, an overview dedicated to the on-demand design of MAs for electrocatalysis is absent. Additionally, the recent research progress for MAs may inspire new insights into this topic. From this perspective, we will first summarize the synthesis of MAs from a historical view. In the following sections, electrocatalysis with MAs for fuel oxidation reactions, oxygen-related reactions, hydrogen-related reactions, and other electrochemical processes will be sequentially discussed. Finally, the challenges and opportunities associated with MAs for electrocatalysis will be summarized to guide the on-target engineering of MAs as efficient electrocatalysts.

2. A Brief Overview of Metal Aerogel Synthesis

Strictly speaking, aerogels are materials derived from a sol-gel process followed by special drying [28]. In this context, special drying usually refers to freeze-drying or supercritical drying, which is used to transfer as-formed wet gels to aerogels. The use of special drying can alleviate the structural collapse incurred by the strong capillary forces generated around the gel network during the drying process, which is realized either by fixing the solid network via freezing (i.e., freeze-drying process) or by transforming the solvent into the supercritical state (i.e., supercritical drying process) before removing it.

MAs are usually defined as free-standing all-metal-made aerogels obtained in the same way as mentioned above. So far, most reported MAs are structured from noble metals, which, however, only account for less than 10% of all metal elements in the periodic table. This is probably because of their relatively higher redox potential compared with other metals, which leads to an easy synthesis, as well as the high stability of the derived noble MAs. Apart from the limited compositions, the synthesis and applications of MAs are also severely hindered by the shortage of structure controllability. As mentioned above, MAs are usually prepared by sequential gelation and drying process. Since the drying method is mature, attention is often paid to the design of the sol-gel process. Usually, depending on whether a separate metal nanoparticle (NP) formation step is involved or not, the gelation methods are divided into two-step and one-step strategies. Following this classification, this section will summarize the state-of-the-art fabrication methods of MAs.

In the early studies on MAs, the two-step strategy was adopted at first, where the sol-gel process undergoes separate metal NP formation and the wet gel formation stage [18,29,30]. Initiated by Bigall et al. in 2009, Au, Ag, Pt, Au-Ag, and Pt-Ag (Figure 1a) aerogels were synthesized by an oxidation-triggered two-step method [18]. In short, the concentrated noble metal NP solutions (the concentration of the metal salts $c_M = 10$ mM) were prepared from a dilute metal salt solution ($c_M = 0.2$ mM) by NaBH_4 -induced reduction followed by ultracentrifugation. After the addition of oxidants (e.g., H_2O_2) or ethanol, NPs spontaneously fused and eventually formed a hydrogel after ~2 weeks. Finally, the corresponding free-standing MAs were obtained by supercritical CO_2 drying. However, the expensive

ultracentrifugation process and long gelation time are not suitable for practical production.

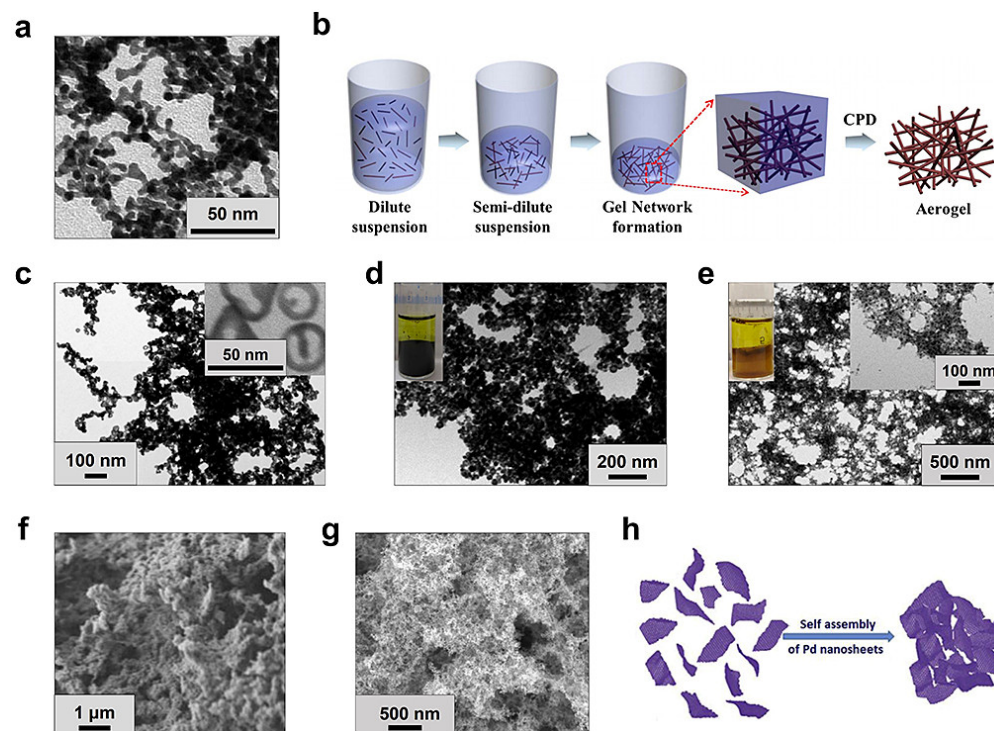


Figure 1. Synthesis of MAs by (a–f) two-step and (g,h) one-step methods. (a) TEM image of a Pt aerogel obtained by using ethanol. Adapted with permission from Ref. [18]. Copyright 2009, Wiley-VCH. (b) Schematic representation of an Ag nanowire (NW) aerogel produced by concentrating the corresponding dilute suspension. Adapted with permission from Ref. [31]. Copyright 2012, Springer Nature. (c) Au/Ag aerogel prepared by concentrated colloidal sols obtained from a rotary evaporation technique; inset shows the individual nanoshell (NS) precursor. Adapted with permission from Ref. [32]. Copyright 2013, American Chemical Society. (d,e) TEM images of aerogels assembled from (24.1 ± 4.5) nm outer diameter Ag NSs; insets show digital photos of the gels induced by applying different amounts of $C(NO_2)_4$. Adapted with permission from Ref. [33]. Copyright 2014, American Chemical Society. (f) Aerogel assembled from Pt nanocubes by using $N_2H_4 \cdot H_2O$. Adapted with permission from Ref. [34]. Copyright 2017, American Chemical Society. (g) $Pt_{50}Pd_{50}$ aerogel synthesized by direct solution-based reduction with $NaBH_4$. Adapted with permission from Ref. [35]. Copyright 2013, Wiley-VCH. (h) Assembly of an aerogel from Pd nanosheets by a CO-bubbling method. Adapted with permission from Ref. [36]. Copyright 2019, Elsevier.

Following the aforementioned study, the two-step strategy has been widely attempted. Apart from initiating gelation by adding oxidants and organic solvents, taking advantage of the salting-out effect, diverse salts (e.g., NaCl, $CaCl_2$, and NH_4F) were successfully used to efficiently induce the gelation process for Au, Ag, Pd, Pt, etc. [32,37–39]. In particular, by adjusting the ion–metal NPs interactions by applying specific salts, the proportion of the isotropic van der Waals attraction force and the anisotropic electrostatic repulsion force could be manipulated, thus leading to Au aerogels with modulated ligament sizes ranging from 6.9 to 113.7 nm [38]. Interestingly, a study reported by Wen et al. found that non-dissociative dopamine can serve as an efficient initiator, capable of producing Au aerogels with a ligament size of as small as ~ 5 nm and a SSA of up to $50.1 \text{ m}^2 \text{ g}^{-1}$ [24]. However, the underlying gelation mechanism is not clear. In a follow-up study by the same group, with the assembly of D-penicillamine-stabilized ultrasmall Au nanoclusters (a diameter of 1.4 nm) with dopamine, the ligament size of the Au aerogels could be further cut down to ~ 3.5 nm [40]. Furthermore, controlled evaporation offers an initiator-free strategy for creating metal gels. As demonstrated by Jung et al., the aqueous suspension of as-prepared

anisotropic 1D Ag NWs can be directly converted into a gel by gradual concentration via controlled evaporation at 313 K (Figure 1b), thus avoiding the introduction of extra impurities [31].

Considering that the NPs' formation and assembly steps are decoupled in the two-step strategy, the NP precursors can be easily engineered before assembly, thus deriving MAs with controlled structures at both nano- and micro-scales [32–34,41–45]. Pioneered by Kulugammana and co-workers in 2013, as-prepared Au-Ag, Pd-Ag, and Pt-Ag alloy NSs were adopted for assembly [32]. As illustrated in Figure 1c, the obtained Au-Ag aerogel displays a hierarchical structure at different scales. In another interesting study, despite the fact that the same precursors (e.g., Ag NSs) were applied, the microstructure and thus the macroscopic transparency of the acquired aerogels could be substantially altered by controlling the etching degree by applying different amounts of $C(NO_2)_4$ (Figure 1d,e) [33]. Concentrating on the Pt system, a study prepared Pt nanocubes and nanospheres in an organic phase before treating them with $N_2H_4 \cdot H_2O$ [34], eventually yielding a hierarchically structured aerogel (Figure 1f). Taking Ni NPs as sacrificial templates, by performing galvanic replacement reaction (GRR) with Pd and/or Pt salts, various Ni-Pd_xPt_y nano-building blocks with hollow spheres or dendrite-like structures were created as precursors [44,45]. Assembling these specific nanostructures leads to the formation of diverse hierarchically structured multi-metallic aerogels. However, the aforementioned strategies usually require a tedious pre-synthesis step for specifically engineered NPs. Besides deliberately shaping NPs, a counterintuitive phenomenon was reported; that is, the spatial element distribution of the resulting bimetallic aerogels is closely dependent on the chemical composition of the NP precursors [46]. It was found that the assembly of Au NPs and Ag NPs, Au NPs and Pd NPs, and Pd NPs and Pt NPs resulted in gels with uniform element distribution, core-shell structure, and separate element domain structures, respectively. This might be attributed to the composition-specific atomic reorganization during the gelation process.

Despite the above achievements, the available morphologies are still limited. On this occasion, when the as-prepared metal gels are regarded as “precursors”, certain complex structures can be created after specific treatment. For example, by performing GRR on a pre-synthesized Ag hydrogel with Pt salts, the derived Pt-Ag bimetallic gel exhibits a unique nanotubular-structured network with thin NWs (~2.6 nm in diameter) as the secondary structure [47]. Another study reported a PdAu-Pt core-shell aerogel by sequential underpotential Cu deposition and GRR [25]. However, these methods often suffer from time-consuming and/or costly processes. Recently, a dynamic-shelling approach was developed by our group, where the semi-finished gel was used as a precursor [22,38,48]. During the fabrication of a bimetallic gel, the “second metal” source was added after the partial gelation of the “first metal”. In this way, the “second metal” will nucleate and grow on the half-formed network of the “first metal”, thus giving rise to core-shell-structured MAs without an additional post-treatment step. This approach may point out a new direction on facile crafting complex structures in MAs.

Although the two-step strategy is advantageous in shaping multiscale structures, it often suffers from high costs and tedious operation. Therefore, the one-step strategy offers a feasible solution. In 2013, a one-step strategy was proposed by Liu and co-workers [35]. Briefly, Pd, Pt, and Pt-Pd gels were obtained from dilute metal salt aqueous solutions after 3–17 days by applying 1.5 equivalents of $NaBH_4$ (Figure 1g). This strategy merges the metal NP formation and the gelation into one step by only applying appropriate reductants, thus considerably simplifying the operation and reducing contamination. Obviously, the core of the one-step strategy lies in the rational selection of the type and the amount of reductants and also provides a comprehensive understanding of the roles played by the reductants in specific scenarios.

Following the first study on the $NaBH_4$ -directed one-step method as described above, an array of reductants, including hydrazine, dimethylamine borane, sodium hypophosphite monohydrate, borane ammonia complex, and glyoxylic acid, were attempted, resulting in MAs based on Au, Ag, Pd, Pt, and Cu [23,36,49–55]. Among them, an interesting study

found that a common organic solvent, i.e., N-methyl pyrrolidone, can function as both a reductant and a nitrogen source during a hydrothermal reaction [55]. The resulting Pt-Cu aerogels feature both a porous structure and unique metal-N bonds. Another study took gas-phase CO as a reductant, where Pd gels structured from 2D Pd nanosheets (thickness of 6.89 nm) were obtained from an acetic acid solution (Figure 1h) [36]. It is claimed that CO can not only reduce the Pd salts, but also serves as a ligand to promote the generation of the Pd nanosheets.

Very recently, our group systematically investigated the roles of NaBH_4 —the most widely used reductant—in the gelation process [23]. It was found that the functions of NaBH_4 depend on the ratio of NaBH_4 to metal (R/M). At a low R/M (<2), all reductants are used for reducing the metal salts, resulting in metal aggregates. A moderate R/M (2–50) leads to a stable metal sol, at which the anions of the products and unreacted reductants can stabilize the as-formed metal NPs. A high R/M (>50) activates the salting-out function of NaBH_4 , causing the formation of metal gels. In particular, an excessive amount of NaBH_4 can substantially promote the gelation process, where a short gelation time of several hours can be realized (vs. several days by other initiating approaches under similar conditions). Furthermore, the high efficiency of NaBH_4 allows the application of various ligands (e.g., trisodium citrate, sodium deoxycholate, β -alanine, and polyvinylpyrrolidone (PVP) for manipulating the behavior of the NP growth, enabling the fabrication of Au aerogels with a small ligament size (~ 4.8 nm) and a large SSA ($59.8 \text{ m}^2 \text{ g}^{-1}$). Meanwhile, single-metallic Ru, Rh, and Os aerogels were also obtained for the first time in the same study. Hence, deep analysis and subtly utilizing the multifunction of reactants (e.g., reductants, initiators, and solvents) are critical for a smart design of MAs.

For both one-step and two-step strategies, conventional studies mostly focus on modulating the reactants. However, it needs to be pointed out that smartly modulating external physical fields may offer a new dimension for controlled synthesis.

From the perspective of modulating the temperature field, an elevated temperature is frequently applied to accelerate the gelation process [51,56–58]. The first study was reported in 2013, where a substantially shortened gelation time was observed for the Au-Ag system from 2–3 weeks at room temperature (298 K) to 12 h at 348 K [56]. By performing gelation at 333 K, Shi et al. reported the quick synthesis of AuPt_x metal hydrogels within 2–4 h (Figure 2a) [57]. Meanwhile, the low-temperature field has also been studied, which can induce gelation and/or shape hierarchical structures [59–68]. For example, by setting a temperature gradient (from 223 K to 263 K) to promote the unidirectional growth of ice crystals, Ag NW aerogels with anisotropic structures and tunable pore sizes were obtained from an Ag NW precursor solution [62]. Starting from highly concentrated metal NP colloids ($c_M > 100 \text{ mM}$), monolithic aerogels (Au, Ag, Pd, and Pt) consisting of self-supported networks can be obtained by freeze-casting (Figure 2b). However, ligands are required to stabilize this high-concentration precursor solution, resulting in residual impurities in the product [63]. To overcome the aforementioned issues, a freeze-thaw method was developed by our group, capable of building hierarchically structured noble-metal gels (e.g., Au, Pd, Rh, Au-Pt, and Au-Rh) directly from low-concentration NP solutions ($c_M \leq 0.5 \text{ mM}$) [67]. As shown in Figure 2c, metal NPs form aggregates (or gel pieces) upon freezing. Then, due to their self-healing property, these aggregates precipitate and link together during the following thawing process, eventually yielding a monolithic gel. In particular, the ligament size of the resulting Au aerogel is as small as $(35.0 \pm 7.2) \text{ nm}$, which is about one order of magnitude thinner than that of the freeze-casting-prepared one (200–500 nm).

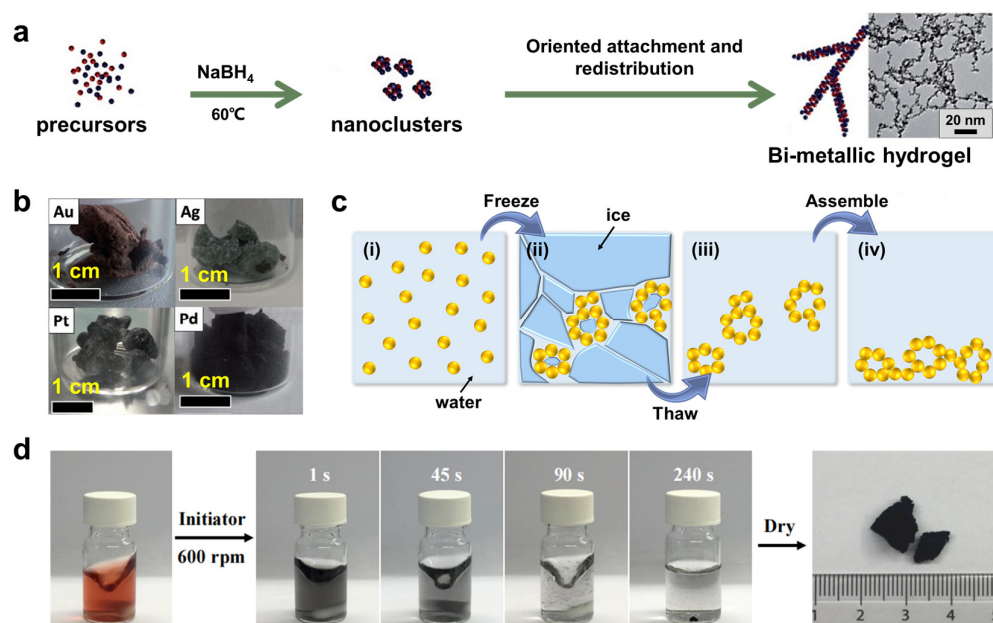


Figure 2. Synthesis of MAs under external fields. (a) Schematic illustration of synthesis of Au-Pt hydrogels under elevated temperature. Adapted with permission from Ref. [57]. Copyright 2017, The Royal Society of Chemistry. (b) Photographs of Au, Ag, Pd, and Pt aerogels prepared by freeze-casting. Adapted with permission from Ref. [63]. Copyright 2016, Wiley-VCH. (c) Proposed mechanism for the freeze-thaw-directed gelation process. Adapted with permission from Ref. [67]. Copyright 2020, Wiley-VCH. (d) The stirring-directed ultrafast gelation of a gold NP solution and the corresponding aerogel. Adapted with permission from Ref. [22]. Copyright 2020, Elsevier.

Furthermore, the influence of external force fields on aerogel synthesis has been studied. To meet practical production times, it is critical to accelerate the slow gelation process in metal systems (several hours to several weeks). To address this issue, our group proposed an unconventional disturbance-directed gelation strategy to accelerate the mass transfer [22,48]. Inspired by the self-healing properties of metal hydrogels, a shearing field generated by stirring was introduced for promoting the mass transfer. After the formation of Au aggregates, the reaction system was left still for gelation via self-healing of the as-formed aggregates (Figure 2d). In this light, the gelation time can be reduced to 1–10 min, which is 2–4 orders of magnitude faster than that reported by conventional methods. It needs to be mentioned that the nature of the self-healing properties of metal hydrogels has not been well understood. Additionally, the feasibility of expansion of such disturbance-directed synthesis tactics to more gel systems should be a meaningful while under-investigated direction.

3. Fuel-Related Electrocatalysis

3.1. Alcohol Oxidation Reaction

Direct alcohol fuel cells, which are fueled by alcohols (e.g., methanol and ethanol), have drawn increasing attention due to their high energy efficiency and low pollution emissions compared with fossil fuels [69]. However, the anodic alcohol oxidation reaction (AOR) is hindered by a high overpotential (η) and sluggish kinetics compared to hydrogen oxidation, thus calling for a new generation of electrocatalysts [70,71]. In this regard, MAs play a critical role due to their excellent performance in the electrocatalytic oxidation of diverse alcohols, including methanol, ethanol, and ethylene glycol. In practice, the design of MAs for AOR can roughly be divided into composition and structure aspects.

Composition design is mostly performed by imparting specific metals or tuning the proportions of different metals, so as to enhance the electrical conductivity and/or modulate the electronic structure [38,44,51,57,58,72–75]. In most studies, Pd- and Pt-based

aerogels are employed for AOR catalysis due to the intrinsically high activity of Pd and Pt. In an early study, α -, β -, or γ -cyclodextrins-modified Pd aerogels were applied for the ethanol oxidation reaction (EOR) [74]. The corresponding forward anodic peak current densities (I_f) normalized by the Pd mass (4.12 to 7.39 A mg⁻¹) are larger than that of commercial Pd/C (3.43 A mg⁻¹), showcasing a higher catalytic activity. The ratios of the peak current densities obtained from forward/backward scans (I_f/I_b) of those aerogels are 1.06 to 1.17 times higher than that of commercial Pd/C, suggesting more efficient oxidation during the forward anodic scan. The high electrocatalytic activity is considered to be the abundant active sites and mass transfer channels of the aerogel, as well as the host–guest interaction between the cyclodextrins and ethanol. Then, a batch of studies were dedicated to enhancing the performance by using bi-/tri-MAs. For instance, by introducing Au and Pt, the resulting Au-Pd and Au-Pd-Pt aerogels exhibit substantially higher performance with I_f of 2.65 and 4.82 A mg_{Pd+Pt}⁻¹, respectively (2.8 to 6.1 times higher than that for commercial Pd/C) [38]. This is rationalized by highly conductive 3D networks offered by gold and potential synergy effects from several metals. Furthermore, considering the cost, inexpensive Cu has also been included [58]. As seen from Figure 3a,b, the Pd₆₈Cu₃₂ aerogel delivers a high forward current density of 3.47 A mg_{Pd}⁻¹ in 1.0 M KOH + 1.0 M ethanol solution, presumably due to its large electrochemically active surface area (37.9 m² g⁻¹, higher than 13.8 m² g⁻¹ of Pd/C).

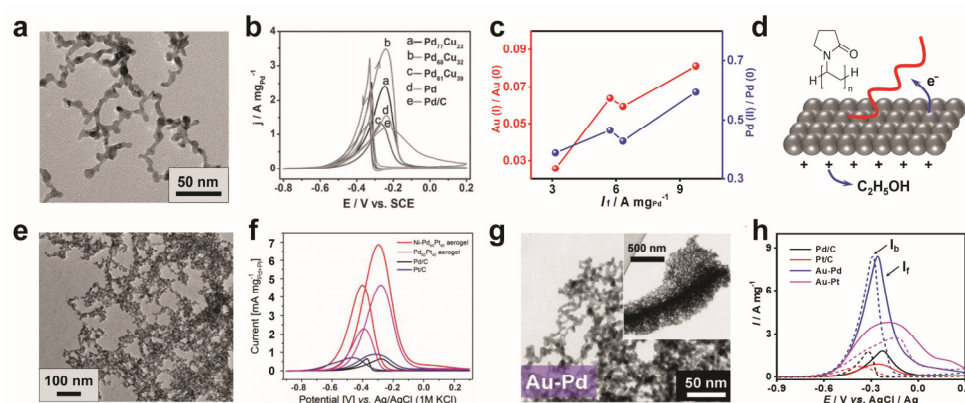


Figure 3. Electrocatalysis towards AOR with MAs. (a–d) Composition design of MAs for EOR. (a,b) TEM image of a PtCu aerogel and current–voltage (CV) measurements of several Pt–Cu aerogels performed in nitrogen-saturated 1.0 M KOH + 1.0 M ethanol solution. Adapted with permission from Ref. [58]. Copyright 2016, Wiley-VCH. (c,d) Ligand-directed modulation for EOR. Correlation between I_f and the valence states of metals for ligand-modified Au–Pd aerogels, and the proposed mechanism of PVP-enhanced ethanol oxidation. (e–h) Structure manipulation of MAs for EOR. Adapted with permission from Ref. [75]. Copyright 2020, Wiley-VCH. (e,f) TEM image of a hierarchically structured Ni–Pd₆₀Pt₄₀ aerogel and CVs performed in 1.0 M NaOH + 1.0 M ethanol solution. Adapted with permission from Ref. [44]. Copyright 2017, Wiley-VCH. (g,h) TEM image of a hierarchically structured Au–Pd aerogel, and CVs performed in 1.0 M KOH + 1.0 M ethanol solution. Adapted with permission from Ref. [67]. Copyright 2020, Wiley-VCH.

Apart from modulating the metal compositions, specific ligands were adopted to adjust the valence state of the aerogels by utilizing the electron charge transfer between the metals and ligands. As shown in Figure 3c,d, a partial electron transfer from the metal to PVP was observed, resulting in a higher surface oxidation state of Au–Pd aerogels and thus promoting the oxidation reaction [75]. In this light, an EOR activity 5.3 times higher than that for Pd/C was realized with the PVP-modified Au–Pd aerogel.

On the other hand, the manipulation of the aerogel structure has been explored at both the nanoscale and the meso-/macroscale to boost the electrocatalytic performance [36,43,44,52,54,67,76]. Bearing a unique core–shell structure at the nanoscale, a Pd₃Pb₁@Pd aerogel shows a high I_f of 6.4 A mg_{Pd}⁻¹ (5.8 times higher than that for

Pd black) towards the ethylene glycol oxidation reaction in 1.0 M KOH + 0.5 M ethylene glycol [54]. In another study, Ni-PdPt aerogels with hollow-spherical and dendritic morphologies at the nanoscale were designed (Figure 3e) [44]. Thanks to the large numbers of accessible catalytic sites, the dendritically structured Ni-Pd₆₀Pt₄₀ aerogel manifests an impressive I_f of 10.6 times higher than with Pd/C (Figure 3f). At the meso-/macroscale, Au-Pd aerogels featuring hierarchically porous structures demonstrate unique advantages (Figure 3g) [67]. As illustrated in Figure 3h, a high I_f of 8.4 A mg⁻¹ was obtained due to a combination of enhanced mass transfer and abundant active sites.

In addition to conventional electrocatalysis, MAs have been recently explored as a photoelectrocatalysis (PEC) platform by utilizing the combined optic and catalytic activities endowed by nanostructured metals. This endeavor was pioneered in 2020 by our group, where the photocatalytic performance for EOR was evaluated with an Au-Pd-Pt aerogel under a white-light LED source (wavelength range of 350–800 nm) (Figure 4a) [22]. As seen from Figure 4b, I_f of the Au-Pd-Pt aerogel raises stepwise from 9.1 to 13.2 A mg_{Pd+Pt}⁻¹ as the light power density increases from 0 to 133 mW cm⁻², which are 5.0 to 7.3 times higher than that of commercial Pd/C in the dark. This light-enhanced performance may be attributed to both the plasmonic absorption of nanostructured noble metals, as well as the photothermal effect from multiple light absorption/scattering inside the gel network. Interestingly, this property may also find applications in sensing. As shown in Figure 4c, switching on/off the light during a chronoamperometry test results in repeated current fluctuations, manifesting a sensitivity of >40.2 μ A mW⁻¹. A follow-up study explored PEC for EOR by using hierarchically structured Au-Pd and Au-Pt aerogels (Figure 4d–f) [67]. Similarly, a ~40% improvement in I_f was observed with an Au-Pd aerogel under irradiation compared with that in the dark (11.8 vs. 8.4 A mg⁻¹), both considerably outperforming that for commercial Pd/C (1.8 A mg⁻¹ in the dark).

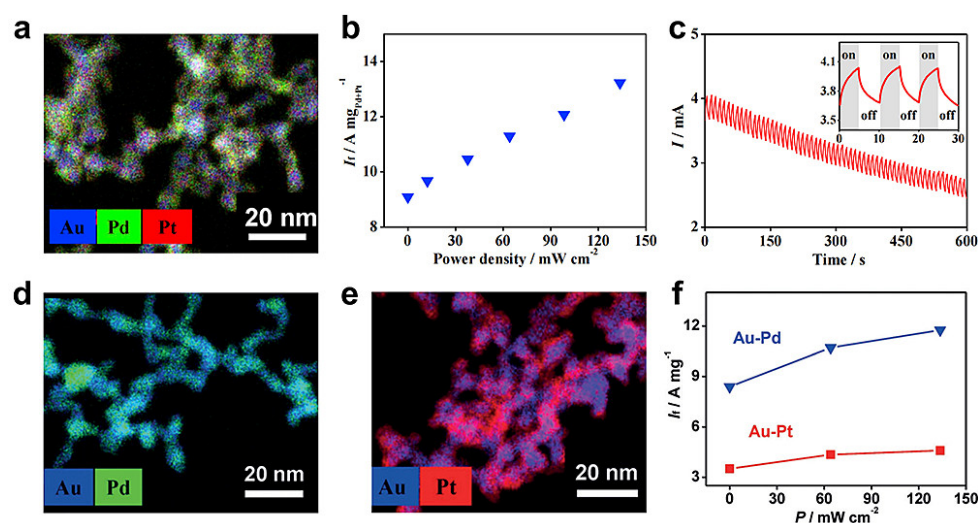


Figure 4. MAs for photoelectrocatalysis. (a–c) Application of an Au-Pd-Pt aerogel for photoelectrocatalysis. Energy-dispersive X-ray spectroscopy (EDXS)-based element distribution, dependence of I_f on the input light power density, and light response behavior. Adapted with permission from Ref. [22]. Copyright 2020, Elsevier. (d–f) EDXS-based element distributions of Au-Pd and Au-Pt aerogels and the dependence of I_f on the input light power density. All tests were performed in nitrogen-saturated 1.0 M KOH + 1.0 M ethanol solution. Adapted with permission from Ref. [67]. Copyright 2020, Wiley-VCH.

3.2. Formic Acid/Formate Oxidation Reaction

FOR has also drawn substantial interest in recent years on account of the high energy density and security of formic acid/formate [77]. MAs have also been applied for electrocatalyzing FOR [47,50,78–81]. In 2018, a Pd-Cu aerogel was reported for efficiently catalyzing formic acid oxidation [50]. In a 0.5 M H₂SO₄ and 0.5 M HCOOH solution, the Pd-Cu

aerogel displayed a high current density of $3.13 \text{ A mg}_{\text{Pd}}^{-1}$, which nearly doubled that of Pd/C ($1.67 \text{ A mg}_{\text{Pd}}^{-1}$). This improved performance can be attributed to the self-supported nature of aerogels, which eliminates the potential carbon substrate corrosion that happens in commercial Pd/C. Recently, an in situ high-potential-driven restructuring strategy was proposed to promote electrocatalytic HCOOK oxidation in alkaline media [80]. As schemed in Figure 5a, the potential cycling of a ternary Ag-Pd-Pt aerogel leads to an outward diffusion of Ag and thus generates amorphous Ag_2O -coupled Pd-Pt on the surface. This architecture can weaken the chemisorption of H_{ad} intermediate because of the lowered d-band center, thus promoting FOR. By cycling Ag-Pd-Pt aerogels between 0.1 V and 1.3 V, the resulting materials exhibit outstanding activity (5 times higher than that for Pd/C) and stability (Figure 5b).

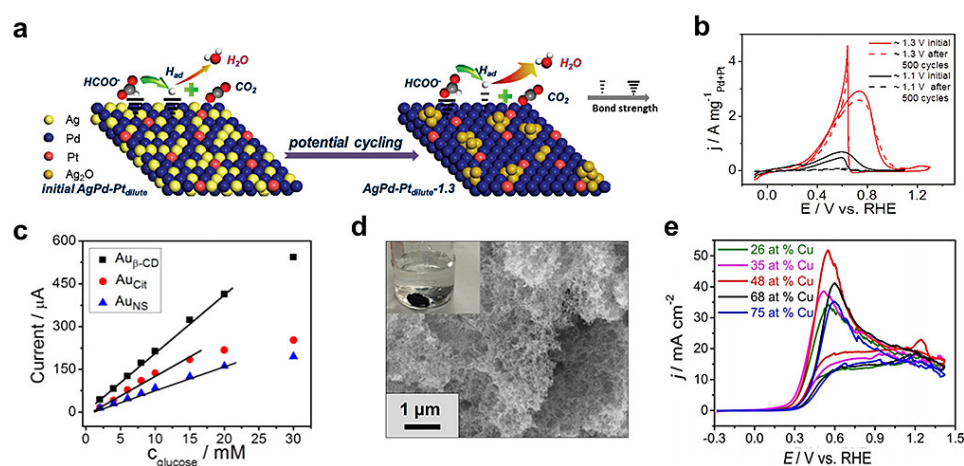


Figure 5. Electrocatalysis towards FOR, GOR, and BOR with MAs. (a,b) FOR with MAs. Schematic illustration of the surface restructuring process of an Ag-Pd-Pt aerogel and stability tests performed in 0.5 M KOH + 0.5 M HCOOK solutions. Adapted with permission from Ref. [80]. Copyright 2019, The Royal Society of Chemistry. (c) GOR catalyzed by different Au aerogels. Adapted with permission from Ref. [24]. Copyright 2016, American Chemical Society. (d,e) BOR with MAs. SEM and a digital photo of an Au₅₂Cu₄₈ aerogel and CVs of different Au-Cu aerogels recorded in a 0.1 M NaBH₄ + 3.0 M NaOH solution. Adapted with permission from Ref. [73]. Copyright 2018, Wiley-VCH.

3.3. Glucose and Borohydride Oxidation Reaction

Glucose is a long-sought-after renewable fuel that can largely advance green energy technologies, and MAs play a critical role in catalyzing the glucose oxidation reaction (GOR) [24,37,40,82]. On the one hand, MAs can act as an auxiliary component to promote the GOR. For example, a Pd aerogel was used as a porous and electrically conductive host to load catalytically active glucose oxidase (GOD) [37]. In this way, mass/electron transfer was enhanced, thus considerably raising the bioelectrocatalytic current compared to that for a bare GOD electrode. On the other hand, MAs can also directly catalyze GOR [24]. As seen in Figure 5c, the current density increases linearly with increasing concentration of glucose from 0 to 20 mM. Particularly, the β -CD-modified Au aerogel displays the highest sensitivity of $(332.9 \pm 7.6) \mu\text{A mM}^{-1}$, which might be attributed to the intermolecular interaction between glucose and β -CD.

Besides the GOR, the borohydride oxidation reaction (BOR) has also been studied recently [73]. As seen from Figure 5d,e, Au-Cu aerogels manifest composition-dependent BOR performance. Among them, the Au₅₂Cu₄₈ aerogel features the most negative onset potential and the highest current density (53 mA cm^{-2}), which is believed to originate from its desirable electronic structure that can excellently balance the borohydride adsorption and intermediate desorption.

4. Oxygen-Related Electrocatalysis

OER and ORR are two oxygen-related electrocatalytic reactions, which are important in the field of energy conversion and storage [83–86]. OER is found as the anodic reaction in water electrolysis, while its large η (usually >300 mV) seriously affects this process [5]. On the other hand, as the cathode reaction in fuel cells and metal-air batteries, ORR is the bottleneck reaction because of its sluggish four-electron transfer process [2]. Commercial OER and ORR catalysts are usually noble-metal-based materials (e.g., Ir- and Ru-based catalysts for OER and Pt-based catalysts for ORR), while their high cost can pose a large constraint for upscaled use. In this regard, MAs may offer unprecedented opportunities by considerably increasing the performance-to-cost ratio for their extended reaction sites and mass transfer highways.

4.1. Oxygen Evolution Reaction

Diverse MAs have been applied for OER catalysis [23,87–89]. As seen in Figure 6a,b, based on the synergy of the highly conductive Au core network and the catalytically active Ir shell, Au-Ir core-shell aerogels manifest a small η (245 mV at 10 mA cm^{-2}) and Tafel slope (36.9 mV dec^{-1}) in 1.0 M KOH , considerably outperforming commercial Ir/C and IrO_2 catalysts ($\eta > 311$ mV and Tafel slope $> 54.3 \text{ mV dec}^{-1}$) [23].

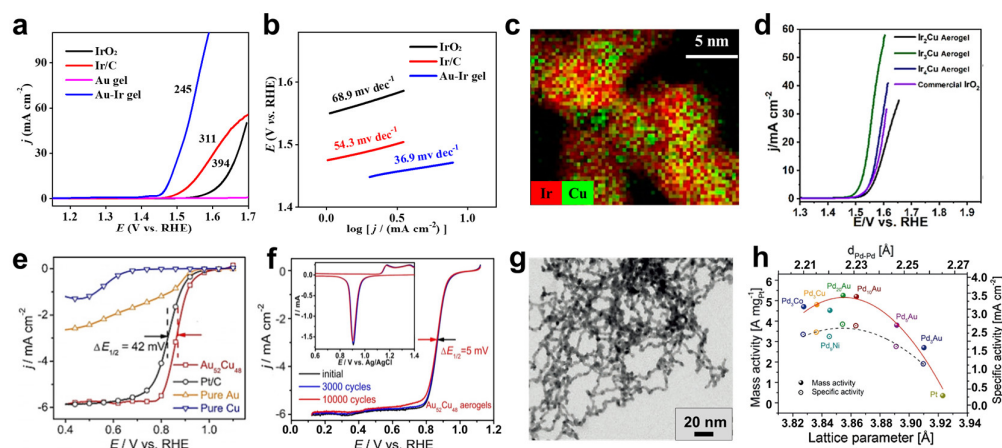


Figure 6. Electrocatalysis for oxygen-related reactions with MAs. (a–d) OER with MAs. (a,b) Polarization curves and Tafel plots of Au aerogels, Au-Ir aerogels, and commercial catalysts performed in N_2 -saturated 1.0 M KOH aqueous solution at 1600 rpm. Adapted with permission from Ref. [23]. Copyright 2020, Nature Publishing Group. (c,d) Electron energy-loss spectroscopy-based element distribution of an Ir_3Cu aerogel and the polarization curves of various Ir_xCu aerogels obtained in O_2 -saturated 0.1 M HClO_4 aqueous solution at 1600 rpm. Adapted with permission from Ref. [88]. Copyright 2018, American Chemical Society. (e–h) ORR with MAs. (e,f) Polarization curves and stability test of an $\text{Au}_{52}\text{Cu}_{48}$ aerogel. Adapted with permission from Ref. [73]. Copyright 2018, Wiley-VCH. (g,h) TEM image of a PdAu-Pt core-shell aerogel as well as the mass activity and specific activity of $\text{Pd}_x\text{M-Pt}$ core-shell aerogels ($\text{M} = \text{Au, Ni, Co, Cu}$) as a function of the lattice parameter of the Pd_xM core aerogels and the Pd-Pd interatomic distance ($d_{\text{Pd-Pd}}$). Adapted with permission from Ref. [25]. Copyright 2018, Wiley-VCH.

To reduce the cost, non-noble metals are introduced into MAs in recent studies. For instance, Ru-Co aerogels were found with high electrical conductivity, as well as abundant active sites, resulting from the presence of oxygen vacancies, thus delivering a small OER η (272 mV at 10 mA cm^{-2}) and Tafel slope (41.6 mV dec^{-1}) in 1.0 M KOH [87]. Another study reported nanovoids-incorporated Ir_xCu aerogels for enhanced OER performance (Figure 6c) [88]. By balancing the binding energy of the oxygen-involved intermediates and the desorption energy of the generated oxygen via tuning the composition, the optimized Ir_3Cu aerogel exhibits the smallest η (298 mV at 10 mA cm^{-2}) in an O_2 -saturated 0.1 M HClO_4 aqueous solution (Figure 6d). Recently, a noble-metal-free Fe-Co-Ni aerogel, as

a cost-effective OER electrocatalyst, was found to deliver an exceptionally low η (235 mV at 10 mA cm⁻²) and a small Tafel slope (50 mV dec⁻¹) in 1.0 M KOH, outperforming that for commercial RuO₂ and thereby offering opportunities towards commercial use [89]. The enhanced performance is due to the synergistic effect of three metals as well as abundant catalytically active structural defects found in the aerogel.

4.2. Oxygen Reduction Reaction

MAs have also been used for catalyzing ORR in recent years, particularly with Pt-based aerogels [35,39,90,91]. The first study was reported in 2013 with Pd-Pt bimetallic aerogels [35]. By tuning the d-band center of the aerogels via modulating the Pd-to-Pt ratio, the optimized Pd₂₀Pt₈₀ aerogel exhibits a 5-times-higher mass activity (1.17 A mg_{Pt+Pd}⁻¹) than that for commercial Pt/C (0.23 A mg_{Pt}⁻¹). By introducing highly conductive Au to enhance the electron transfer, the acquired Au-Pt aerogel delivers an impressive pH-universal ORR catalytic performance, exhibiting a high specific activity (>3 times compared with that for Pt/C) and stability in both 0.1 M KOH and 0.1 M HClO₄ aqueous solutions [39]. Inspired by the outstanding ORR catalytic performance of Pt-Ni nanostructures [92], Pt-Ni aerogels were fabricated as cathode catalysts for fuel cells, showcasing both excellent specific activity (0.2 mA cm_{Pt}⁻² at 0.95 V_{RHE} under acidic conditions, which is 3 times higher than that for Pt/C) and stability (~10% decrease in mass activity at 0.9 V_{RHE} after 10,000 potential cycles) [90,91]. Furthermore, Pt-free MAs, such as Au-Cu aerogels, were also investigated [73]. As seen from Figure 6e,f, the charge transfer from Cu to Au can lower the d-band center of Au, thus the resulting in the Au₅₂Cu₄₈ aerogel displaying a more positive onset potential compared with commercial Pt/C (1.00 V and 0.96 V vs. RHE, respectively) and sustaining high specific activity (0.891 mA cm⁻²) and mass activity (0.920 A mg_{Au}⁻¹) after 10,000 potential cycles. This is presumably associated with the superior stability provided by the Au component.

On the other hand, structure engineering of MAs can also enhance the ORR performance. For example, taking advantage of the synergy of the highly conductive Au core network and the Pt₃Pd shell, a specially designed Au@Pt₃Pd core-shell aerogel was shown to deliver much higher mass activity and specific activity (0.812 A mg_{Pt+Pd}⁻¹ and 24.3 mA cm⁻²) than that for commercial Pt/C (0.412 A mg_{Pt}⁻¹ and 10.5 mA cm⁻²) at 0.85 V vs. RHE [42]. Core-shell-structured Pd_xAu-Pt aerogels, consisting of an ultrathin Pt shell and a composition-tunable Pd_xAu core, were also explored as electrocatalysts [25]. By manipulating the lattice strain through designing the lattice mismatch between the outer Pt and various core metals, the optimized PdAu-Pt core-shell aerogel exhibits incredible mass activity and specific activity of 5.25 A mg_{Pt}⁻¹ and 2.53 mA cm⁻², which are 18.7- and 4.1 times higher than those of Pt/C (Figure 6g,h).

5. Hydrogen-Related Electrocatalysis

Electrocatalysis with hydrogen can be divided into two classes, i.e., the hydrogen oxidation reaction and the hydrogen evolution reaction. The eco-friendly HOR process acts as the anodic reaction in hydrogen fuel cells, while the HER process is the cathodic reaction in the electrochemical water splitting that is critical for hydrogen production.

5.1. Hydrogen Oxidation Reactions

So far, electrocatalytic HOR has been only sporadically studied with MAs. As seen from Figure 7a, 2D lamellar Pt-Rh nanoalloy aerogels (NAAs) made up of ultrathin interweaved NWs were reported [93]. The authors claimed that strong electronic coupling between Pt and Rh can weaken the hydrogen binding energy (Figure 7b), thus leading to a lower half-wave potential ($E_{1/2}$) of 17 mV, as well as the highest specific activity and mass activity (5.5 and 2.6 times higher than that of commercial Pt/C, respectively, at η = 50 mV) among all tested catalysts (Figure 7c,d).

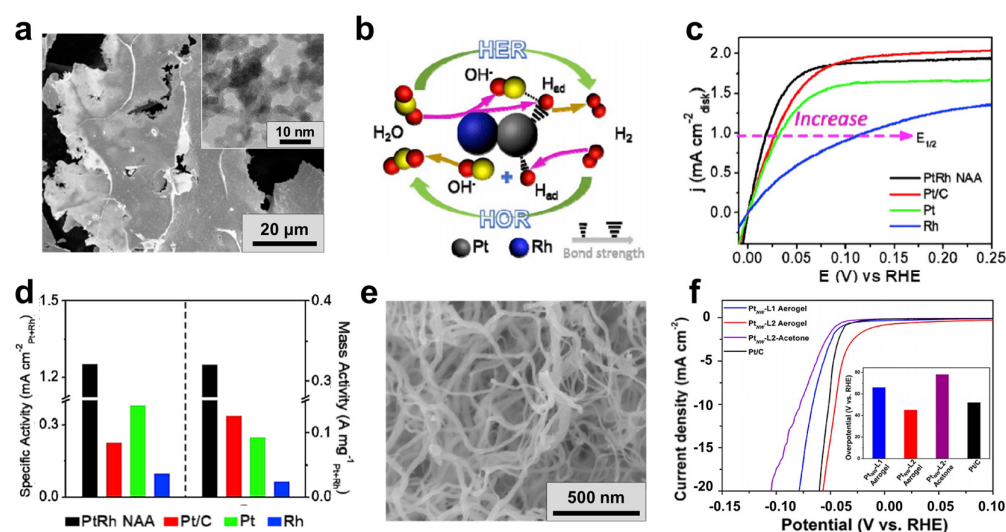


Figure 7. Electrocatalysis for hydrogen-related reactions with MAs. (a–d) HOR with a lamellar Pt₆₈Rh₃₂ aerogel. SEM image (inset: TEM image), proposed catalytic mechanisms, polarization curves, and normalized activities (at $\eta = 50$ mV) of a Pt₆₈Rh₃₂ aerogel performed in H₂-saturated 0.1 M KOH solution under 1600 rpm. Adapted with permission from Ref. [93]. Copyright 2019, Elsevier. (e,f) HER with Pt NW aerogels. SEM image of the Pt_{NW}-L2 aerogel and polarization curves of various catalysts. Adapted with permission from Ref. [94]. Copyright 2019, American Chemical Society.

5.2. Hydrogen Evolution Reactions

Recently, MAs were also extensively studied for HER [39,93–95]. In terms of the structure, besides HOR catalysis, 2D-sheets-assembled Pt-Rh NAAs also perform well towards alkaline HER, exhibiting a smaller η of 55 mV at 10 mA cm⁻², as well as a 2.3-times-higher mass activity in 1.0 M KOH solution compared to Pt/C [93]. In another study, by grafting two kinds of ligands (L1 and L2) bearing thiol and glutamic acid moieties on Pt NWs for controlled assembly, the resulting aerogels displayed different HER performances [94]. The strong self-assembling ability of L2 renders the Pt_{NW}-L2 aerogels (Figure 7e) with an optimized performance (the lowest η of 45 mV at 10 mA cm⁻²) among the tested materials (Figure 7f), but the specific reason is unclear. On the other hand, the smart design of the composition also plays a critical role. By screening various bimetallic systems, Au-Rh aerogels were found to deliver the smallest η (18–22 mV at 10 mA cm⁻²) and Tafel slopes (29–47 mV) at different pH values (pH = 0–14), considerably outperforming commercial Pt/C catalysts [39]. However, a clear explanation is absent.

6. Electrocatalysis in Other Processes

Apart from the above examples, MAs have also been involved in various other important electrocatalytic processes, such as the CO₂ reduction reaction (CO₂RR) and the nitrate reduction reaction.

Electrochemical CO₂RR provides a promising way of meeting current energy demands and reducing greenhouse gas emissions by producing value-added chemicals with renewable electricity. MAs also play a critical role in this field [48,96–99]. Lu et al. reported the first study on CO₂RR with Mas [97]. By regulating the composition of bimetallic Pd-Cu aerogels, the Pd₈₃Cu₁₇ aerogel with the highest (Cu^I + Cu⁰)/Cu^{II} ratio displayed the best performance, with a faradaic efficiency of 80.0% at a current density of 31.8 mA cm⁻² for CH₃OH production in 1-butyl-3-methylimidazolium tetrafluoroborate aqueous solution. The excellent performance is rationalized by the efficient adsorption of CO_{ads} and CHO_{ads} on Cu^I + Cu⁰ species. From the structure aspect, a well-defined Au-Pd core-shell aerogel (Figure 8a) was found to efficiently promote CO₂ activation while suppressing H₂ activation evolution compared to common Au-Pd aerogels as suggested by both experimental and

theoretical studies (Figure 8b,c), thus manifesting outstanding Faradaic efficiency of up to 99.96% for CO selectivity and sustaining a $FE_{CO} > 98\%$ at $\eta = 390$ mV over 12 h [48].

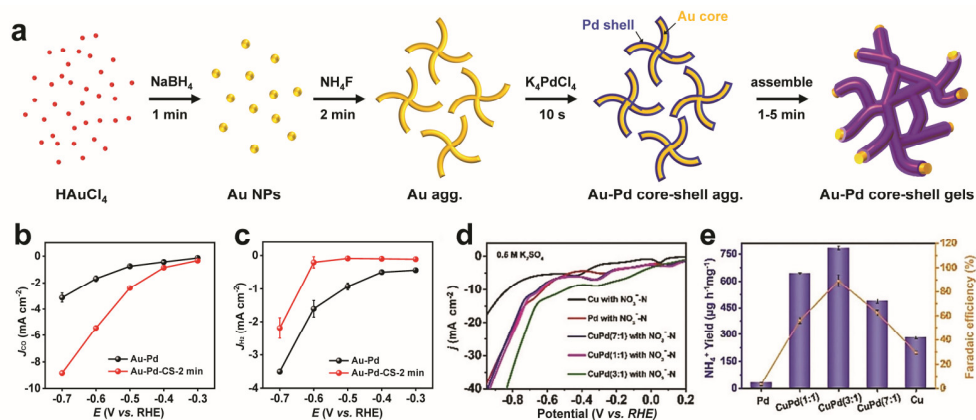


Figure 8. Electrocatalysis for other reactions with MAs. (a–c) CO_2RR with MAs. Synthesis process of core-shell-structured Au-Pd aerogels, and the corresponding CO and H_2 partial current densities versus the applied potential in 0.1 M KHCO_3 . Adapted with permission from Ref. [48]. Copyright 2021, The Royal Society of Chemistry. (d,e) Nitrate-to-ammonia conversion with Cu-Pd bimetallic aerogels. Polarization curves performed in $0.5 \text{ M K}_2\text{SO}_4$, and NH_3 yield rates, as well as faradaic efficiencies for various catalysts. Adapted with permission from Ref. [100]. Copyright 2021, The Royal Society of Chemistry.

Besides CO_2 conversion, a growing level of nitrate (NO_3^-) places another potential threat to the environment. To address it, Cu-rich Cu-Pd bimetallic aerogels were developed by choosing Pd as the active metal and Cu as the promoting metal [100]. Among all tested catalysts (Figure 8d,e), the Cu-Pd (3:1) aerogel stands out for the enhanced hydrogen adsorption at Pd-sites and the well-tuned d-band center of Cu. In this light, a high NO_3^- conversion rate (95.27%), ammonia selectivity (77.49%), and ammonia faradaic efficiency (90.02%) at 0.46 V vs. RHE were acquired. The superior performance could be attributed to the abundant catalytically active sites provided by the aerogel structure as well as the synergy of Cu and Pd.

7. Conclusions and Perspectives

The last decade witnessed the discovery and prosperous development of MAs as well as their widespread applications in electrocatalysis. As one of the latest members in the aerogel family, MAs have proved highly desirable for diverse applications, including catalysis, optical devices, and sensing. Meanwhile, the uniqueness of MAs also brings about quite a few challenges.

Fundamentally, the distinctive properties of metals (e.g., high mass density, plasticity, and delocalized electrons) lead to abnormal gelation behavior compared to conventional gel systems. Despite tremendous efforts devoted, a general and unambiguous understanding of the physical picture of the gelation process is still absent, thus restricting investigations of controlled synthesis as well as properties. For the following five or more years, it is expected that the development of the synthesis methodology, the enrichment of the material basis, and the exploration of basic physicochemical properties of MAs are sought-after directions in this field.

Practically, it is accepted that the most promising application of MAs at present is electrocatalysis based on the combined effects of a highly conductive network, large SSA, and abundant active sites. Principles for performance optimization can be summarized into composition tuning (for enhancing the conductivity and adjusting the electronic structure) and structure tuning (for increasing accessible sites). Currently, most studies concentrate on noble metal systems, which inevitably raises the cost. Additionally, quite a few studies only superficially demonstrate catalytic performance without investigating underlying

mechanisms, which contributes little to the development of practical applications. Thirdly, the aerogel form seems useless under the conventional catalyst preparation process (grinding and dispersing). The subtle utilization of the free-standing feature of MAs needs to be considered when applied for electrocatalysis and beyond. Finally, the unique features of metals are still less explored. Our group has pioneered photoelectrocatalysis with MAs by taking advantage of their optical properties, while more attributes of metals and MAs are waiting to be discovered.

To sum up, as a class of cutting-edge materials, MAs deserve much more attention due to unsolved fundamental challenges and broad application perspectives. Researchers with multi-disciplinary backgrounds ranging from chemistry, materials science, physics, and biology are welcome to jointly explore this young and promising field.

Funding: This research was funded by the National Natural Science Foundation of China (22202009, 52201262), College Students' Innovation and Entrepreneurship Training Program (BIT2022LH122), Natural Science Foundation of Shandong Province (ZR2022QE001), and Guangdong Basic and Applied Basic Research Foundation (2021A1515110920).

Acknowledgments: The support from the Experimental Center of Advanced Materials in Beijing Institute of Technology is acknowledged.

Conflicts of Interest: The authors declare no conflict of interest.

References

- Cong, Y.; Yi, B.; Song, Y. Hydrogen oxidation reaction in alkaline media: From mechanism to recent electrocatalysts. *Nano Energy* **2018**, *44*, 288–303. [\[CrossRef\]](#)
- Katsounaros, I.; Cherevko, S.; Zeradjanin, A.R.; Mayrhofer, K.J.J. Oxygen Electrochemistry as a Cornerstone for Sustainable Energy Conversion. *Angew. Chem. Int. Ed.* **2014**, *53*, 102–121. [\[CrossRef\]](#)
- Wu, X.; Wang, Y.; Wu, Z.-S. Design principle of electrocatalysts for the electrooxidation of organics. *Chem* **2022**, *8*, 2294–2629. [\[CrossRef\]](#)
- Wang, Y.; Wang, D.; Li, Y. A fundamental comprehension and recent progress in advanced Pt-based ORR nanocatalysts. *SmartMat* **2021**, *2*, 56–75. [\[CrossRef\]](#)
- Song, J.; Wei, C.; Huang, Z.-F.; Liu, C.; Zeng, L.; Wang, X.; Xu, Z.J. A review on fundamentals for designing oxygen evolution electrocatalysts. *Chem. Soc. Rev.* **2020**, *49*, 2196–2214. [\[CrossRef\]](#)
- Zheng, Y.; Jiao, Y.; Jaroniec, M.; Qiao, S.Z. Advancing the Electrochemistry of the Hydrogen-Evolution Reaction through Combining Experiment and Theory. *Angew. Chem. Int. Ed.* **2015**, *54*, 52–65. [\[CrossRef\]](#)
- Lu, T.; Li, T.; Shi, D.; Sun, J.; Pang, H.; Xu, L.; Yang, J.; Tang, Y. In situ establishment of Co/MoS₂ heterostructures onto inverse opal-structured N,S-doped carbon hollow nanospheres: Interfacial and architectural dual engineering for efficient hydrogen evolution reaction. *SmartMat* **2021**, *2*, 591–602. [\[CrossRef\]](#)
- Birdja, Y.Y.; Pérez-Gallent, E.; Figueiredo, M.C.; Göttle, A.J.; Calle-Vallejo, F.; Koper, M.T.M. Advances and challenges in understanding the electrocatalytic conversion of carbon dioxide to fuels. *Nat. Energy* **2019**, *4*, 732–745. [\[CrossRef\]](#)
- Wang, N.; Miao, R.K.; Lee, G.; Vomiero, A.; Sinton, D.; Ip, A.H.; Liang, H.; Sargent, E.H. Suppressing the liquid product crossover in electrochemical CO₂ reduction. *SmartMat* **2021**, *2*, 12–16. [\[CrossRef\]](#)
- Du, R.; Zhang, N.; Zhu, J.; Wang, Y.; Xu, C.; Hu, Y.; Mao, N.; Xu, H.; Duan, W.; Zhuang, L.; et al. Nitrogen-Doped Carbon Nanotube Aerogels for High-Performance ORR Catalysts. *Small* **2015**, *11*, 3903–3908. [\[CrossRef\]](#)
- Zhang, J.; Xia, Z.; Dai, L. Carbon-based electrocatalysts for advanced energy conversion and storage. *Sci. Adv.* **2015**, *1*, e1500564. [\[CrossRef\]](#) [\[PubMed\]](#)
- Cai, B.; Eychmüller, A. Promoting Electrocatalysis upon Aerogels. *Adv. Mater.* **2019**, *31*, 1804881. [\[CrossRef\]](#)
- Majidi, L.; Yasaei, P.; Warburton, R.E.; Fuladi, S.; Cavin, J.; Hu, X.; Hemmat, Z.; Cho, S.B.; Abbasi, P.; Voros, M.; et al. New Class of Electrocatalysts Based on 2D Transition Metal Dichalcogenides in Ionic Liquid. *Adv. Mater.* **2019**, *31*, e1804453. [\[CrossRef\]](#)
- Du, R.; Wu, Y.; Yang, Y.; Zhai, T.; Zhou, T.; Shang, Q.; Zhu, L.; Shang, C.; Guo, Z. Porosity Engineering of MOF-Based Materials for Electrochemical Energy Storage. *Adv. Energy Mater.* **2021**, *11*, 2100154. [\[CrossRef\]](#)
- Hu, X.; Sun, Z.; Mei, G.; Zhao, X.; Xia, B.Y.; You, B. Engineering Nonprecious Metal Oxides Electrocatalysts for Two-Electron Water Oxidation to H₂O₂. *Adv. Energy Mater.* **2022**, *12*, 2201466. [\[CrossRef\]](#)
- Li, J.; Li, H.; Xu, L.; Wang, L.; Hu, Z.; Liu, L.; Huang, Y.; Kotov, N.A. Biomimetic nanoporous aerogels from branched aramid nanofibers combining high heat insulation and compressive strength. *SmartMat* **2021**, *2*, 76–87. [\[CrossRef\]](#)
- Leventis, N.; Chandrasekaran, N.; Sotiriou-Leventis, C.; Mumtaz, A. Smelting in the age of nano: Iron aerogels. *J. Mater. Chem.* **2009**, *19*, 63–65. [\[CrossRef\]](#)
- Bigall, N.C.; Herrmann, A.K.; Vogel, M.; Rose, M.; Simon, P.; Carrillo-Cabrera, W.; Dorfs, D.; Kaskel, S.; Gaponik, N.; Eychmüller, A. Hydrogels and aerogels from noble metal nanoparticles. *Angew. Chem. Int. Ed.* **2009**, *48*, 9731–9734. [\[CrossRef\]](#)

19. Liu, W.; Herrmann, A.-K.; Bigall, N.C.; Rodriguez, P.; Wen, D.; Oezaslan, M.; Schmidt, T.J.; Gaponik, N.; Eychmüller, A. Noble Metal Aerogels Synthesis, Characterization, and Application as Electrocatalysts. *Acc. Chem. Res.* **2015**, *48*, 154–162. [\[CrossRef\]](#)
20. Du, R.; Fan, X.; Jin, X.; Hübner, R.; Hu, Y.; Eychmüller, A. Emerging Noble Metal Aerogels: State of the Art and a Look Forward. *Matter* **2019**, *1*, 39–56. [\[CrossRef\]](#)
21. Du, R.; Jin, X.; Hübner, R.; Fan, X.; Hu, Y.; Eychmüller, A. Engineering Self-Supported Noble Metal Foams Toward Electrocatalysis and Beyond. *Adv. Energy Mater.* **2020**, *10*, 1901945. [\[CrossRef\]](#)
22. Du, R.; Joswig, J.-O.; Fan, X.; Hübner, R.; Spittel, D.; Hu, Y.; Eychmüller, A. Disturbance-Promoted Unconventional and Rapid Fabrication of Self-Healable Noble Metal Gels for (Photo-)Electrocatalysis. *Matter* **2020**, *2*, 908–920. [\[CrossRef\]](#)
23. Du, R.; Wang, J.; Wang, Y.; Hübner, R.; Fan, X.; Senkovska, I.; Hu, Y.; Kaskel, S.; Eychmüller, A. Unveiling Reductant Chemistry in Fabricating Noble Metal Aerogels for Superior Oxygen Evolution and Ethanol Oxidation. *Nat. Commun.* **2020**, *11*, 1590. [\[CrossRef\]](#)
24. Wen, D.; Liu, W.; Haubold, D.; Zhu, C.; Oschatz, M.; Holzschuh, M.; Wolf, A.; Simon, F.; Kaskel, S.; Eychmüller, A. Gold aerogels: Three-dimensional assembly of nanoparticles and their use as electrocatalytic interfaces. *ACS Nano* **2016**, *10*, 2559–2567. [\[CrossRef\]](#) [\[PubMed\]](#)
25. Cai, B.; Hübner, R.; Sasaki, K.; Zhang, Y.; Su, D.; Ziegler, C.; Vukmirovic, M.B.; Rellinghaus, B.; Adzic, R.R.; Eychmüller, A. Core-Shell Structuring of Pure Metallic Aerogels towards Highly Efficient Platinum Utilization for the Oxygen Reduction Reaction. *Angew. Chem. Int. Ed.* **2018**, *57*, 2963–2966. [\[CrossRef\]](#) [\[PubMed\]](#)
26. Wang, H.; Fang, Q.; Gu, W.; Du, D.; Lin, Y.; Zhu, C. Noble Metal Aerogels. *ACS Appl. Mater. Interfaces* **2020**, *12*, 52234–52250. [\[CrossRef\]](#) [\[PubMed\]](#)
27. Jiang, X.; Du, R.; Hübner, R.; Hu, Y.; Eychmüller, A. A Roadmap for 3D Metal Aerogels: Materials Design and Application Attempts. *Matter* **2021**, *4*, 54–94. [\[CrossRef\]](#)
28. Alemán, J.; Chadwick, A.V.; He, J.; Hess, M.; Horie, K.; Jones, R.G.; Kratochvíl, P.; Meisel, I.; Mita, I.; Moad, G. Definitions of terms relating to the structure and processing of sols, gels, networks, and inorganic-organic hybrid materials (IUPAC Recommendations 2007). *Pure Appl. Chem.* **2007**, *79*, 1801–1829. [\[CrossRef\]](#)
29. Graham, T.X. Liquid diffusion applied to analysis. *Philos. Trans. R. Soc. Lond.* **1861**, *151*, 183–224. [\[CrossRef\]](#)
30. Sun, H.; Xu, Z.; Gao, C. Multifunctional, Ultra-Flyweight, Synergistically Assembled Carbon Aerogels. *Adv. Mater.* **2013**, *25*, 2554–2560. [\[CrossRef\]](#)
31. Jung, S.M.; Jung, H.Y.; Dresselhaus, M.S.; Jung, Y.J.; Kong, J. A facile route for 3D aerogels from nanostructured 1D and 2D materials. *Sci. Rep.* **2012**, *2*, 849. [\[CrossRef\]](#) [\[PubMed\]](#)
32. Ranmohotti, K.G.; Gao, X.; Arachchige, I.U. Salt-Mediated Self-Assembly of Metal Nanoshells into Monolithic Aerogel Frameworks. *Chem. Mater.* **2013**, *25*, 3528–3534. [\[CrossRef\]](#)
33. Gao, X.; Esteves, R.J.; Luong, T.T.H.; Jaini, R.; Arachchige, I.U. Oxidation-Induced Self-Assembly of Ag Nanoshells into Transparent and Opaque Ag Hydrogels and Aerogels. *J. Am. Chem. Soc.* **2014**, *136*, 7993–8002. [\[CrossRef\]](#) [\[PubMed\]](#)
34. Naskar, S.; Freytag, A.; Deutsch, J.; Wendt, N.; Behrens, P.; Köckritz, A.; Bigall, N.C. Porous Aerogels from Shape-Controlled Metal Nanoparticles Directly from Nonpolar Colloidal Solution. *Chem. Mater.* **2017**, *29*, 9208–9217. [\[CrossRef\]](#)
35. Liu, W.; Rodriguez, P.; Borchardt, L.; Foelske, A.; Yuan, J.; Herrmann, A.K.; Geiger, D.; Zheng, Z.; Kaskel, S.; Gaponik, N. Bimetallic Aerogels: High-Performance Electrocatalysts for the Oxygen Reduction Reaction. *Angew. Chem. Int. Ed.* **2013**, *52*, 9849–9852. [\[CrossRef\]](#)
36. Zareie Yazdan-Abad, M.; Noroozifar, M.; Douk, A.S.; Modarresi-Alam, A.R.; Saravani, H. Shape engineering of palladium aerogels assembled by nanosheets to achieve a high performance electrocatalyst. *Appl. Catal. B-Environ.* **2019**, *250*, 242–249. [\[CrossRef\]](#)
37. Wen, D.; Herrmann, A.-K.; Borchardt, L.; Simon, F.; Liu, W.; Kaskel, S.; Eychmüller, A. Controlling the growth of palladium aerogels with high-performance toward bioelectrocatalytic oxidation of glucose. *J. Am. Chem. Soc.* **2014**, *136*, 2727–2730. [\[CrossRef\]](#)
38. Du, R.; Hu, Y.; Hübner, R.; Joswig, J.-O.; Fan, X.; Eychmüller, A. Specific Ion Effects Directed Noble Metal Aerogels: Versatile Manipulation for Electrocatalysis and Beyond. *Sci. Adv.* **2019**, *5*, eaaw4590. [\[CrossRef\]](#)
39. Du, R.; Jin, W.; Hübner, R.; Zhou, L.; Hu, Y.; Eychmüller, A. Engineering Multimetallic Aerogels for pH-Universal HER and ORR Electrocatalysis. *Adv. Energy Mater.* **2020**, *10*, 1903857. [\[CrossRef\]](#)
40. Xu, J.; Sun, F.; Li, Q.; Yuan, H.; Ma, F.; Wen, D.; Shang, L. Ultrasmall Gold Nanoclusters-Enabled Fabrication of Ultrafine Gold Aerogels as Novel Self-Supported Nanozymes. *Small* **2022**, *18*, 2200525. [\[CrossRef\]](#)
41. Gao, X.; Esteves, R.J.A.; Nahar, L.; Nowaczyk, J.; Arachchige, I.U. Direct Cross-Linking of Au/Ag Alloy Nanoparticles into Monolithic Aerogels for Application in Surface-Enhanced Raman Scattering. *ACS Appl. Mater. Interfaces* **2016**, *8*, 13076–13085. [\[CrossRef\]](#) [\[PubMed\]](#)
42. Shi, Q.; Zhu, C.; Li, Y.; Xia, H.; Engelhard, M.H.; Fu, S.; Du, D.; Lin, Y. A Facile Method for Synthesizing Dendritic Core-Shell Structured Ternary Metallic Aerogels and Their Enhanced Electrochemical Performances. *Chem. Mater.* **2016**, *28*, 7928–7934. [\[CrossRef\]](#)
43. Shi, Q.; Zhu, C.; Tian, M.; Su, D.; Fu, M.; Engelhard, M.H.; Chowdhury, I.; Feng, S.; Du, D.; Lin, Y. Ultrafine Pd ensembles anchored-Au₂Cu aerogels boost ethanol electrooxidation. *Nano Energy* **2018**, *53*, 206–212. [\[CrossRef\]](#)

44. Cai, B.; Dianat, A.; Hübner, R.; Liu, W.; Wen, D.; Benad, A.; Sonntag, L.; Gemming, T.; Cuniberti, G.; Eychmüller, A. Multimetallic Hierarchical Aerogels: Shape Engineering of the Building Blocks for Efficient Electrocatalysis. *Adv. Mater.* **2017**, *29*, 1605254. [CrossRef]
45. Cai, B.; Wen, D.; Liu, W.; Herrmann, A.K.; Benad, A.; Eychmüller, A. Function-Led Design of Aerogels: Self-Assembly of Alloyed PdNi Hollow Nanospheres for Efficient Electrocatalysis. *Angew. Chem. Int. Ed.* **2015**, *54*, 13101–13105. [CrossRef]
46. Kühn, L.; Herrmann, A.K.; Rutkowski, B.; Oezaslan, M.; Nachtegaal, M.; Klose, M.; Giebeler, L.; Gaponik, N.; Eckert, J.; Schmidt, T.J. Alloying Behavior of Self-Assembled Noble Metal Nanoparticles. *Chem. Eur. J.* **2016**, *22*, 13446–13450. [CrossRef]
47. Liu, W.; Haubold, D.; Rutkowski, B.; Oschatz, M.; Hubner, R.; Werheid, M.; Ziegler, C.; Sonntag, L.; Liu, S.; Zheng, Z. Self-Supporting Hierarchical Porous PtAg Alloy Nanotubular Aerogels as Highly Active and Durable Electrocatalysts. *Chem. Mater.* **2016**, *28*, 6477–6483. [CrossRef]
48. Du, R.; Jin, W.; Wu, H.; Hübner, R.; Zhou, L.; Xue, G.; Hu, Y.; Eychmüller, A. Rapid synthesis of gold–palladium core–shell aerogels for selective and robust electrochemical CO₂ reduction. *J. Mater. Chem. A* **2021**, *9*, 17189–17197. [CrossRef]
49. Burpo, F.J.; Nagelli, E.A.; Morris, L.A.; McClure, J.P.; Ryu, M.Y.; Palmer, J.L. Direct solution-based reduction synthesis of Au, Pd, and Pt aerogels. *J. Mater. Res.* **2017**, *32*, 4153–4165. [CrossRef]
50. Douk, A.S.; Farsadrooh, M.; Damanigol, F.; Moghaddam, A.A.; Saravani, H.; Noroozifar, M. Porous three-dimensional network of Pd–Cu aerogel toward formic acid oxidation. *RSC Adv.* **2018**, *8*, 23539–23545. [CrossRef]
51. Douk, A.S.; Saravani, H.; Noroozifar, M. Three-dimensional assembly of building blocks for the fabrication of Pd aerogel as a high performance electrocatalyst toward ethanol oxidation. *Electrochim. Acta* **2018**, *275*, 182–191. [CrossRef]
52. Yazdan-Abad, M.Z.; Noroozifar, M.; Alam, A.R.M.; Saravani, H. Palladium aerogel as a high-performance electrocatalyst for ethanol electro-oxidation in alkaline media. *J. Mater. Chem. A* **2017**, *5*, 10244–10249. [CrossRef]
53. Zeng, Y.; Li, Y.; Tan, X.; Gong, J.; Wang, Z.; An, Y.; Wang, Z.; Li, H. B,N-Doped PdRu Aerogels as High-Performance Peroxidase Mimics for Sensitive Detection of Glucose. *ACS Appl. Mater. Interfaces* **2021**, *13*, 36816–36823. [CrossRef] [PubMed]
54. Zhu, C.; Shi, Q.; Fu, S.; Song, J.; Du, D.; Su, D.; Engelhard, M.H.; Lin, Y. Core-shell PdPb@Pd aerogels with multiply-twinned intermetallic nanostructures: Facile synthesis with accelerated gelation kinetics and their enhanced electrocatalytic properties. *J. Mater. Chem. A* **2018**, *6*, 7517–7521. [CrossRef]
55. Song, T.; Xue, H.; Sun, J.; Guo, N.; Sun, J.; Wang, Q. Solvent assistance induced surface N-modification of PtCu aerogels and their enhanced electrocatalytic properties. *Chem. Commun.* **2021**, *57*, 7140–7143. [CrossRef] [PubMed]
56. Herrmann, A.-K.; Formanek, P.; Borchardt, L.; Klose, M.; Giebeler, L.; Eckert, J.; Kaskel, S.; Gaponik, N.; Eychmüller, A. Multimetallic aerogels by template-free self-assembly of Au, Ag, Pt, and Pd nanoparticles. *Chem. Mater.* **2013**, *26*, 1074–1083. [CrossRef]
57. Shi, Q.; Zhu, C.; Du, D.; Bi, C.; Xia, H.; Feng, S.; Engelhard, M.H.; Lin, Y. Kinetically controlled synthesis of AuPt bi-metallic aerogels and their enhanced electrocatalytic performances. *J. Mater. Chem. A* **2017**, *5*, 19626–19631. [CrossRef]
58. Zhu, C.; Shi, Q.; Fu, S.; Song, J.; Xia, H.; Du, D.; Lin, Y. Efficient synthesis of MCu (M = Pd, Pt, and Au) aerogels with accelerated gelation kinetics and their high electrocatalytic activity. *Adv. Mater.* **2016**, *28*, 8779–8783. [CrossRef] [PubMed]
59. Muller, D.; Zambo, D.; Dorfs, D.; Bigall, N.C. Cryoaerogels and Cryohydrogels as Efficient Electrocatalysts. *Small* **2021**, *17*, e2007908. [CrossRef]
60. Zambo, D.; Rusch, P.; Lubkemann, F.; Bigall, N.C. Noble-Metal Nanorod Cryoaerogels with Electrocatalytically Active Surface Sites. *ACS Appl. Mater. Interfaces* **2021**, *13*, 57774–57785. [CrossRef]
61. Tang, Y.; Yeo, K.L.; Chen, Y.; Yap, L.W.; Xiong, W.; Cheng, W. Ultralow-density copper nanowire aerogel monoliths with tunable mechanical and electrical properties. *J. Mater. Chem. A* **2013**, *1*, 6723–6726. [CrossRef]
62. Gao, H.L.; Xu, L.; Long, F.; Pan, Z.; Du, Y.X.; Lu, Y.; Ge, J.; Yu, S.H. Macroscopic Free-Standing Hierarchical 3D Architectures Assembled from Silver Nanowires by Ice Templating. *Angew. Chem. Int. Ed.* **2014**, *53*, 4561–4566. [CrossRef] [PubMed]
63. Freytag, A.; Sánchez-Paradinas, S.; Naskar, S.; Wendt, N.; Colombo, M.; Pugliese, G.; Poppe, J.; Demirci, C.; Kretschmer, I.; Bahnmann, D.W.; et al. Versatile Aerogel Fabrication by Freezing and Subsequent Freeze-Drying of Colloidal Nanoparticle Solutions. *Angew. Chem. Int. Ed.* **2016**, *55*, 1200–1203. [CrossRef] [PubMed]
64. Gilbert, D.A.; Burks, E.C.; Ushakov, S.V.; Abellan, P.; Arslan, I.; Felter, T.E.; Navrotsky, A.; Liu, K. Tunable Low Density Palladium Nanowire Foams. *Chem. Mater.* **2017**, *29*, 9814–9818. [CrossRef]
65. Qian, F.; Lan, P.C.; Freyman, M.C.; Chen, W.; Kou, T.; Olson, T.Y.; Zhu, C.; Worsley, M.A.; Duoss, E.B.; Spadaccini, C.M.; et al. Ultralight Conductive Silver Nanowire Aerogels. *Nano Lett.* **2017**, *17*, 7171–7176. [CrossRef]
66. Fears, T.M.; Hammons, J.A.; Sain, J.D.; Nielsen, M.H.; Braun, T.; Kucheyev, S.O. Ultra-low-density silver aerogels via freeze-substitution. *APL Mater.* **2018**, *6*, 091103. [CrossRef]
67. Du, R.; Joswig, J.-O.; Hübner, R.; Zhou, L.; Wei, W.; Hu, Y.; Eychmüller, A. Freeze-Thaw-Promoted Fabrication of Clean and Hierarchically-Structured Noble Metal Aerogels for Electrocatalysis and Photoelectrocatalysis. *Angew. Chem. Int. Ed.* **2020**, *59*, 8293–8300. [CrossRef]
68. Qian, F.; Troksa, A.; Fears, T.M.; Nielsen, M.H.; Nelson, A.J.; Baumann, T.F.; Kucheyev, S.O.; Han, T.Y.-J.; Bagge-Hansen, M. Gold Aerogel Monoliths with Tunable Ultralow Densities. *Nano Lett.* **2020**, *20*, 131–135. [CrossRef]
69. Elsaid, K.; Abdelfatah, S.; Abdel Elabsir, A.M.; Hassiba, R.J.; Ghouri, Z.K.; Vechot, L. Direct alcohol fuel cells: Assessment of the fuel's safety and health aspects. *Int. J. Hydrogen Energy* **2021**, *46*, 30658–30668. [CrossRef]

70. Fu, X.; Wan, C.; Huang, Y.; Duan, X. Noble Metal Based Electrocatalysts for Alcohol Oxidation Reactions in Alkaline Media. *Adv. Funct. Mater.* **2022**, *32*, 2106401. [\[CrossRef\]](#)
71. Yang, N.; Chen, D.; Cui, P.; Lu, T.; Liu, H.; Hu, C.; Xu, L.; Yang, J. Heterogeneous nanocomposites consisting of Pt₃Co alloy particles and CoP₂ nanorods towards high-efficiency methanol electro-oxidation. *SmartMat* **2021**, *2*, 234–245. [\[CrossRef\]](#)
72. Nahar, L.; Farghaly, A.A.; Esteves, R.J.A.; Arachchige, I.U. Shape Controlled Synthesis of Au/Ag/Pd Nanoalloys and Their Oxidation-Induced Self-Assembly into Electrocatalytically Active Aerogel Monoliths. *Chem. Mater.* **2017**, *29*, 7704–7715. [\[CrossRef\]](#)
73. Wang, J.; Chen, F.; Jin, Y.; Johnston, R.L. Gold–Copper Aerogels with Intriguing Surface Electronic Modulation as Highly Active and Stable Electrocatalysts for Oxygen Reduction and Borohydride Oxidation. *ChemSusChem* **2018**, *11*, 1354–1364. [\[CrossRef\]](#)
74. Liu, W.; Herrmann, A.K.; Geiger, D.; Borchardt, L.; Simon, F.; Kaskel, S.; Gaponik, N.; Eychmüller, A. High-Performance Electrocatalysis on Palladium Aerogels. *Angew. Chem. Int. Ed.* **2012**, *51*, 5743–5747. [\[CrossRef\]](#) [\[PubMed\]](#)
75. Fan, X.; Zerebecki, S.; Du, R.; Hübner, R.; Marzum, G.; Jiang, G.; Hu, Y.; Barcikowski, S.; Reichenberger, S.; Eychmüller, A. Promoting the Electrocatalytic Performance of Noble Metal Aerogels by Ligand-Directed Modulation. *Angew. Chem. Int. Ed.* **2020**, *59*, 5706–5711. [\[CrossRef\]](#) [\[PubMed\]](#)
76. Slater, A.G.; Cooper, A.I. Function-led design of new porous materials. *Science* **2015**, *348*, aaa8075. [\[CrossRef\]](#) [\[PubMed\]](#)
77. Rice, C.; Ha, S.; Masel, R.I.; Waszczuk, P.; Wieckowski, A.; Barnard, T. Direct formic acid fuel cells. *J. Power Source* **2002**, *111*, 83–89. [\[CrossRef\]](#)
78. Tang, S.; Vongehr, S.; Wang, Y.; Cui, J.; Wang, X.; Meng, X. Versatile synthesis of high surface area multi-metallic nanosponges allowing control over nanostructure and alloying for catalysis and SERS detection. *J. Mater. Chem. A* **2014**, *2*, 3648–3660. [\[CrossRef\]](#)
79. Douk, A.S.; Saravani, H.; Yazdan Abad, M.Z.; Noroozifar, M. Controlled organization of building blocks to prepare three-dimensional architecture of Pd–Ag aerogel as a high active electrocatalyst toward formic acid oxidation. *Compos. B Eng.* **2019**, *172*, 309–315. [\[CrossRef\]](#)
80. Wang, J.; Chen, F.; Jin, Y.; Guo, L.; Gong, X.; Wang, X.; Johnston, R.L. In situ high-potential-driven surface restructuring of ternary AgPd–Pt dilute aerogels with record-high performance improvement for formate oxidation electrocatalysis. *Nanoscale* **2019**, *11*, 14174–14185. [\[CrossRef\]](#)
81. Wang, Q.; Chen, F.; Guo, L.; Jin, T.; Liu, H.; Wang, X.; Gong, X.; Liu, Y. Nanoalloying effects on the catalytic activity of the formate oxidation reaction over AgPd and AgCuPd aerogels. *J. Mater. Chem. A* **2019**, *7*, 16122–16135. [\[CrossRef\]](#)
82. Wen, D.; Liu, W.; Herrmann, A.K.; Eychmüller, A. A membraneless glucose/O₂ biofuel cell based on Pd aerogels. *Chem. Eur. J.* **2014**, *20*, 4380–4385. [\[CrossRef\]](#)
83. Lori, O.; Zion, N.; Honig, H.C.; Elbaz, L. 3D Metal Carbide Aerogel Network as a Stable Catalyst for the Hydrogen Evolution Reaction. *ACS Catal.* **2021**, *11*, 13707–13713. [\[CrossRef\]](#)
84. Zion, N.; Douglin, J.C.; Cullen, D.A.; Zelenay, P.; Dekel, D.R.; Elbaz, L. Porphyrin Aerogel Catalysts for Oxygen Reduction Reaction in Anion-Exchange Membrane Fuel Cells. *Adv. Funct. Mater.* **2021**, *31*, 2100963. [\[CrossRef\]](#)
85. Moschkowitsch, W.; Zion, N.; Honig, H.C.; Levy, N.; Cullen, D.A.; Elbaz, L. Mixed-Metal Nickel–Iron Oxide Aerogels for Oxygen Evolution Reaction. *ACS Catal.* **2022**, *12*, 12162–12169. [\[CrossRef\]](#)
86. Zion, N.; Peles-Strahl, L.; Friedman, A.; Cullen, D.A.; Elbaz, L. Electrocatalysis of Oxygen Reduction Reaction in a Polymer Electrolyte Fuel Cell with a Covalent Framework of Iron Phthalocyanine Aerogel. *ACS Appl. Energy Mater.* **2022**, *5*, 7997–8003. [\[CrossRef\]](#)
87. Lin, Z.; Liu, S.; Liu, Y.; Liu, Z.; Zhang, S.; Zhang, X.; Tian, Y.; Tang, Z. Rational design of Ru aerogel and RuCo aerogels with abundant oxygen vacancies for hydrogen evolution reaction, oxygen evolution reaction, and overall water splitting. *J. Power Source* **2021**, *514*, 230600. [\[CrossRef\]](#)
88. Shi, Q.; Zhu, C.; Zhong, H.; Su, D.; Li, N.; Engelhard, M.H.; Xia, H.; Zhang, Q.; Feng, S.; Beckman, S.P.; et al. Nanovoid Incorporated Irx Cu Metallic Aerogels for Oxygen Evolution Reaction Catalysis. *ACS Energy Lett.* **2018**, *3*, 2038–2044. [\[CrossRef\]](#)
89. Yan, S.; Zhong, M.; Wang, C.; Lu, X. Amorphous aerogel of trimetallic FeCoNi alloy for highly efficient oxygen evolution. *Chem. Eng. J.* **2022**, *430*, 132955. [\[CrossRef\]](#)
90. Henning, S.; Ishikawa, H.; Kühn, L.; Herranz, J.; Müller, E.; Eychmüller, A.; Schmidt, T.J. Unsupported Pt–Ni Aerogels with Enhanced High Current Performance and Durability in Fuel Cell Cathodes. *Angew. Chem. Int. Ed.* **2017**, *56*, 10707–10710. [\[CrossRef\]](#)
91. Henning, S.; Kühn, L.; Herranz, J.; Durst, J.; Binninger, T.; Nachtegaal, M.; Werheid, M.; Liu, W.; Adam, M.; Kaskel, S. Pt–Ni aerogels as unsupported electrocatalysts for the oxygen reduction reaction. *J. Electrochem. Soc.* **2016**, *163*, F998–F1003. [\[CrossRef\]](#)
92. Huang, X.; Zhao, Z.; Cao, L.; Chen, Y.; Zhu, E.; Lin, Z.; Li, M.; Yan, A.; Zettl, A.; Wang, Y.M.; et al. High-performance transition metal-doped Pt₃Ni octahedra for oxygen reduction reaction. *Science* **2015**, *348*, 1230–1234. [\[CrossRef\]](#) [\[PubMed\]](#)
93. Jin, Y.; Chen, F.; Wang, J.; Guo, L.; Jin, T.; Liu, H. Lamellar platinum–rhodium aerogels with superior electrocatalytic performance for both hydrogen oxidation and evolution reaction in alkaline environment. *J. Power Source* **2019**, *435*, 226798. [\[CrossRef\]](#)
94. Zheng, Y.; Li, N.; Mukherjee, S.; Yang, Y.; Yan, J.; Liu, J.; Fang, Y. A Versatile Strategy for Tailoring Noble Metal Supramolecular Gels/Aerogels and Their Application in Hydrogen Evolution. *ACS Appl. Nano Mater.* **2019**, *2*, 3012–3020. [\[CrossRef\]](#)
95. Lu, Q.; Yu, Y.; Ma, Q.; Chen, B.; Zhang, H. 2D Transition-Metal-Dichalcogenide-Nanosheet-Based Composites for Photocatalytic and Electrocatalytic Hydrogen Evolution Reactions. *Adv. Mater.* **2016**, *28*, 1917–1933. [\[CrossRef\]](#)
96. Yan, S.; Mahyoub, S.A.; Lin, J.; Zhang, C.; Hu, Q.; Chen, C.; Zhang, F.; Cheng, Z.J.N. Au aerogel for selective CO₂ electroreduction to CO: Ultrafast preparation with high performance. *Mater. Sci.* **2021**, *33*, 125705. [\[CrossRef\]](#)

97. Lu, L.; Sun, X.; Ma, J.; Yang, D.; Wu, H.; Zhang, B.; Zhang, J.; Han, B. Highly Efficient Electroreduction of CO₂ to Methanol on Palladium–Copper Bimetallic Aerogels. *Angew. Chem. Int. Ed.* **2018**, *57*, 14149–14153. [[CrossRef](#)]
98. Wang, W.; Gong, S.; Liu, J.; Ge, Y.; Wang, J.; Lv, X. Ag-Cu aerogel for electrochemical CO₂ conversion to CO. *J. Colloid Interface Sci.* **2021**, *595*, 159–167. [[CrossRef](#)]
99. Wu, Z.; Wu, H.; Cai, W.; Wen, Z.; Jia, B.; Wang, L.; Jin, W.; Ma, T. Engineering Bismuth-Tin Interface in Bimetallic Aerogel with a 3D Porous Structure for Highly Selective Electrocatalytic CO₂ Reduction to HCOOH. *Angew. Chem. Int. Ed. Engl.* **2021**, *60*, 12554–12559. [[CrossRef](#)]
100. Xu, Y.; Ren, K.; Ren, T.; Wang, M.; Liu, M.; Wang, Z.; Li, X.; Wang, L.; Wang, H. Cooperativity of Cu and Pd active sites in CuPd aerogels enhances nitrate electroreduction to ammonia. *Chem. Commun.* **2021**, *57*, 7525–7528. [[CrossRef](#)]

Disclaimer/Publisher’s Note: The statements, opinions and data contained in all publications are solely those of the individual author(s) and contributor(s) and not of MDPI and/or the editor(s). MDPI and/or the editor(s) disclaim responsibility for any injury to people or property resulting from any ideas, methods, instructions or products referred to in the content.